THE XIONG'AN NEW AREA DEFORMATION MONITORING USING SENTINEL-1 SAR DATA BASED ON SBAS-INSAR TECHNIQUE

Xiaoqing Wang, Peng Zhang, Junli Wu*, Zhanyi Sun, Qinglan Zhang*

National Geomatics Center of China, Beijng, China-(xqwang, pzhang, szy, jlwu, qlzhang) @ngcc.cn

KEY WORDS: Xiong'an New Area, deformation, 2017 to 2020, sentinel-1, SBAS-InSAR.

ABSTRACT:

In order to study the land subsidence trend since the construction of the Xiong'an New Area, 125 images of Sentinel-1 from January 2017 to September 2020 was obtained in this paper, and the average land subsidence rate and cumulative land subsidence of Xiong'an New Area is obtained by the SBAS-InSAR technology of multi-main image coherent target by GAMMA and the Self-developed software, and the causes of land subsidence from the geographical space in the Xiong'an New Area were analyzed by the divisional timing analysis method. The results showed that about 80% of Xiong'an New Area had slight land subsidence with the rate less than 1cm/yr and the cumulative subsidence less than 3cm, and the maximum subsidenc occurred in the northern of Xiongxian County with rate 7cm/yr and the cumulative subsidence was 30cm. Furthermore, the average subsidence rate and the cumulative maximum subsidence in the north and the northwest of Xiongxian County, the Baima Village and the Beifeng Village were studied. The research results showed that the land subsidence in Xiong'an New Area was related to the over exploitation of geothermal resources and groundwater, and the results could provide important reference values for keep abreast of the land subsidence status of the Xiong'an New Area, as well as the healthy development and long-term planning of the New Area.

1. INTRODUCTION

On April 1, 2017, the government of China decided to establish a national new area of Xiong'an in the hinterland of North China around Xiongxian County, Anxin County and the Baiyangdian area of Rongcheng. With the goal of relieving non-capital functions of Beijing, the basic construction of Xiong'an New Area includes external transportation, urban transportation, construction of above-ground and underground buildings, as well as the development and utilization of groundwater and geothermal resources. However, due to the relatively flat and low-lying terrain, the hinterland of North China, where the new area located, has a sedimentary layer of great thickness and an aquifer holds rich water (ZHANG Y H et al,2011). Moreover, the shallow surface is soft, with large pores and strong compressibility (ZHANG Ling et al,2020. As a result, huge engineering construction in a short time, especially the large-scale exploitation of underground resources and deep utilization of underground space, will definitely lead to a wide range of subsidence and affect the construction of the new area and its sustainable development.

Synthetic aperture radar interferometry (InSAR) measurement technology is a new remote sensing technology that can effectively monitor slight land deformation (Wang Xiaoqing et al,2018). Compared with traditional monitoring technology, InSAR technology has the advantages of wide coverage, all-weather and low cost, and it has been applied to urban land subsidence monitoring. Foreign scholars Ferretti et al. proposed time-series analysis techniques such as PS-InSAR and SBAS-InSAR to improve the reliability of deformation monitoring (GAO Ertao et al,2019). SBAS-InSAR technology selects images with short time baselines in multiple images acquired and combines them into several small sets, conducting deformation monitoring even with a small number of images. Furthermore, it can greatly reduce the de-coherence between interfering images and take all coherent point information into account when remove the atmospheric phase, leading to better atmospheric phase removal effect.

With the rapid development of cities and the increase of population, the geothermal and groundwater resources in the North China Plain such as Beijing (Yang Q et al,2018), Tianjin and Hebei have been exploited continuously (Jia Sanman et al,2019), resulting in large-scale land subsidence. For example, based on SBAS-InSAR technology, Ge Daqing and others obtained the information of ground subsidence in the North China Plain from 2012 to 2015 with RADA-SAT-2 data. However, the land subsidence in Xiongxian County, Rongcheng County, Anxin County and Gaoyang County has not been described specifically. Before the construction of the New Area, Zhang Yonghong et al. got the data of land subsidence of Xiong'an from 2012 to 2016 with the same technology. The results show that during this period, about 78% of the area of Xiong'an New Area was in the land subsidence area with the subsidence rate of about 10mm per year, and the area where the risk of land subsidence was evaluated as relatively serious and serious were concentrated in Xiongxian County. DAIKR et al. monitored the land subsidence in the first year of construction (2017-2018) of the Xiong'an New Area, and pointed out that the distribution of land subsidence in this area was closely related to the spatial distribution of thermal well mining.

To sum up, a large range of land subsidence is founded in the Xiong'an New Area according to the existing research results of land subsidence, and its development trend and its relationship with the distribution of underground resource exploitation are worthy of further exploration with the deepening of resource exploitation during the construction of the New Area. Therefore, based on the SBAS-InSAR technology, this paper monitors the land subsidence in the area with the Sentinel-1 data from 2017 to 2020, obtains the change rate and cumulative subsidence of the four key areas since the construction of the New Area,

* Corresponding author

analyzes the relationship between land subsidence and geothermal resource exploitation, agricultural irrigation and industrial water consumption, providing important reference values for keep abreast of the land subsidence status of the Xiong'an New Area, as well as the healthy development and long-term planning of the New Area.

2. RESEARCH AREA AND DATA

2.1 Research Area

Xiong'an New Area is a national New Area in Hebei Province and locates in the North China Plain, and adjacent to Beijing, Tianjin and Baoding. It covers a total area of 1576.6 km2, and still lacks of fresh water resources though with Baiyangdian, Xiaoyi River, Fuhe, Caohe and other water systems. After the establishment of the Xiong'an New Area, a large number of infrastructures have been built, and due to the long-term over-exploitation of groundwater, the North China Plain is truly troubled with land subsidence and the research area with relatively serious problem is shown in Figure 1.

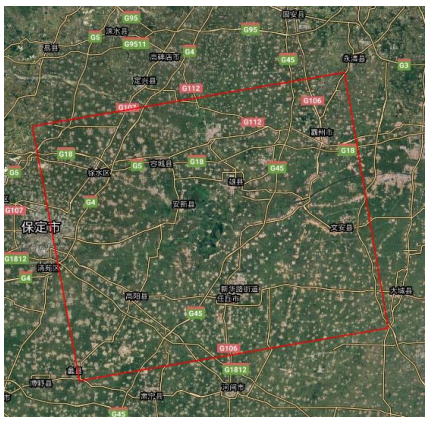

Figure 1. study area

2.2 Experimental Data

The situation of land subsidence of Xiong'an New Area during 2017-2020 was monitored based on SBAS-InSAR technology and with Sentinel-1 (1W) data to keep abreast of land subsidence in the area. The technology and tools used in the paper includes: Sentinel-1 interferometric image of the European Space Agency; C-band (wavelength 5.6cm) with resolution of 5m×20m; single-polarization (VV) observation method with the interference mode width of 250km×250km and the resolution of 30m(XIONG Peng et al,2020); TOPS mode imaging, which could provide high-quality and wide-range interference phase values(XIONG Jiacheng et al,2019). The basic parameter information of Sentinel-1 image data is shown in Table 1.

Parameter	Value
Access to satellite	Sentinel-1B
Orbit	Inbound pass
Resolution / (m x m)	5 x 20
Radar wavelength / cm	5.6
Polarization mode	VV
Revisit period / d	12
Angle of incidence/ (°)	39.1
Image time	2017-06—2019-08
Number of images/scenes	32

Table 1. Basic parameter information of Sentinel-1B 1W mode image data

The Sentinel-1 satellite is a two-constellation satellite with a revisit period that can be shortened to 6 days. In this research, the Sentinel-1 data of 125 scenes that covering the research area was used, and its time span was from January 8, 2017 to September 1, 2020. The number of data sources and time distribution are shown in Figure 2.

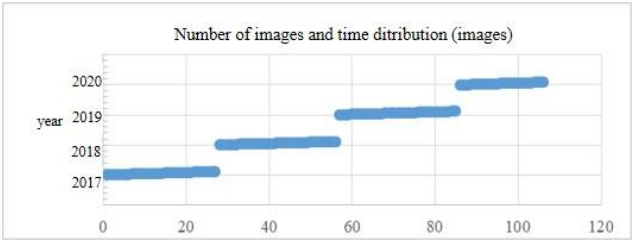

Figure 2. Number of data sources and time distribution

In this paper, the precise orbit ephemerides (POD) of the Sentinel-1 satellite was used for orbital error correction; NASA 30-meter resolution Shuttle Radar Topography Mission (SRTM) data was used as an external reference DEM to remove terrain effects.

3. DATA PROCESSING AND RESULT ANALYSIS

3.1 Process Flow

Small baseline subset interferometry (SBAS-InSAR) , proposed by P. Berardino, is a new time-series analysis method for monitoring small land deformation and it can effectively overcome the limiting factors (space-time de-coherence, atmospheric effects, etc.) in the data processing of the differential interferometric synthetic aperture radar (D-InSAR) measurement technology (Solari L et al,2016), and continuously monitor the microdeformation of and with accuracy of millimeter level. The technical flow of SBAS-InSAR is shown in Figure 3.

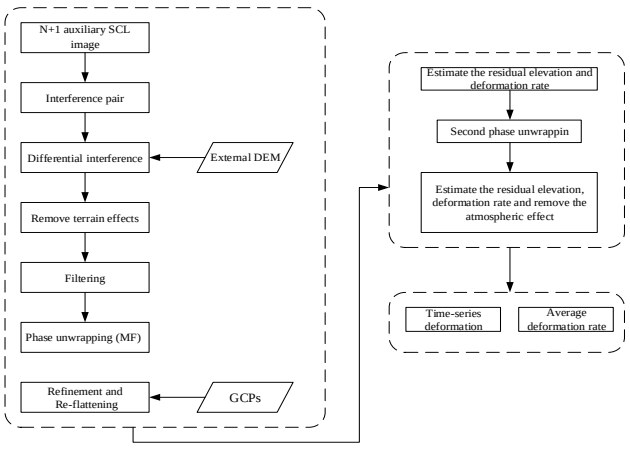

Figure 3. SBAS-InSAR data processing process

Extract the average subsidence rate and cumulative subsidence of the Xiong'an New Area and its surrounding areas with obtained radar image data processed by GAMMA and SBAS-InSAR technology that based on multi-main image coherent targets, and extract average subsidence rate and cumulative subsidence with self-developed deformation analysis program.

In addition, crop the SAR image in sub-areas to improve calculation speed and accuracy of monitoring results since the coverage area of Sentinel-1 interferometric wide image is (250×250) km, which is much larger than the research area in this paper. Then the data processing and deformation analysis of sub-areas were completed under the same standard. A unified deformation reference benchmark was established for different sub-areas to conduct overall integration analysis that across tracks and multiple areas, then the deformation rates and cumulative deformation were analysed overall and sub-areas.

3.2 Interference Processing

Select any scene of the Sentinel-1 interferometric wide images as the super main image, register the rest images with the super main image, and set the temporal baseline threshold (TBT) and perpendicular baseline threshold (PBT) . N+1 SAR images can generate at most M differential interferograms, and satisfy the following relational equations:

$$\frac{N+1}{2} \leq M \leq N(\frac{N+1}{2}) \quad , \tag{1}$$

Analyze the temporal baseline and perpendicular baseline distance, and set the maximum temporal interval baseline threshold as 36d and the perpendicular baseline threshold as 149, forming 197 interference image pairs. The baseline spatiotemporal distribution formed by the interference pair is shown in Figure 4.

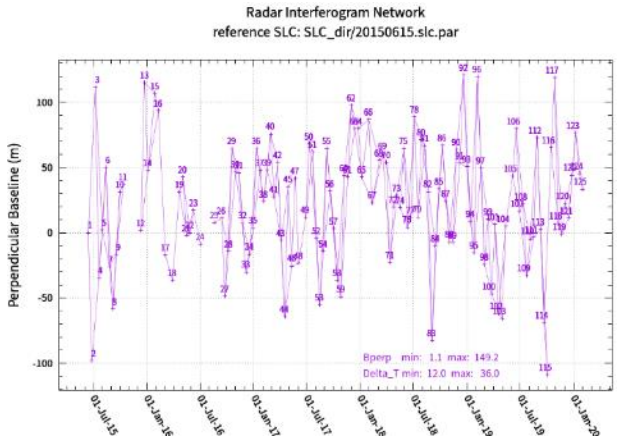

Figure 4. Baseline spatiotemporal distribution of small baseline pair

Conduct interference processing to main and auxiliary images according to the combination of small baseline pair to generate differential interference phase (as shown in Figure 5 and Figure 6). There is a lot of noise in the original differential interferogram, which seriously interferes with the efficiency and accuracy of the two-dimensional phase unwrapping algorithm and the accuracy of extracting deformation information. While the noise is significantly reduced by filtering, and the fringes are relatively clear.

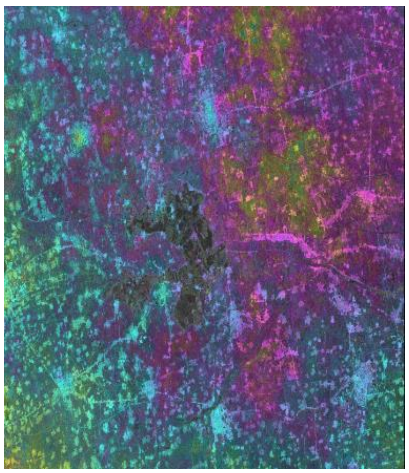

Figure 5. Original differential interference phase

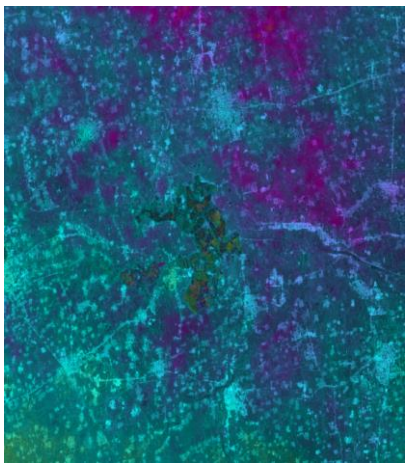

Figure 6. Filtered differential interference phase

3.3 Subsidence time-series Analysis

The surface deformation can be decomposed into linear deformation (main deformation) and nonlinear residual deformation (Zhu L et al,2015), and the interference phase difference formed by two coherent points (set as m, n) on the i-th interferogram can be expressed as (WANG Xiaoqing et al,2012):

$$\Delta\varphi_{m,n}(T^i) = \Delta\delta_{m,n}(T^i) + \Delta\beta_{m,n}(T^i) + \Delta\alpha_{m,n}(T^i) + \Delta N_{m,n}(T^i), \tag{2}$$

$$\Delta\delta_{m,n}(T^i) = \frac{4\pi}{\lambda} T^i \Delta v_{m,n} + \frac{4\pi}{\lambda} \frac{TB_m^i}{R_{m\sin\theta_m^i}^i} \Delta h_{m,n} \quad , \tag{3}$$

where $\Delta\varphi_{m,n}$ (T^i) is the differential interference phase difference of adjacent highly coherent points, T^i is the time baseline of the interferogram, $\Delta\delta_{m,n}(T^i)$ is the model phase difference of adjacent highly coherent points, including the shared phases of difference in elevation error between bright spots ($\Delta h_{m,n}$) and the difference in linear phase transition rate ($\Delta v_{m,n}$), $\Delta\beta_{m,n}$ (T^i) is the difference between nonlinear deformation phases, $\Delta\alpha_{m,n}$ (T^i) is the atmospheric influence phase difference, $\Delta N_{m,n}(T^i)$ is the noise phase difference, λ is the radar wavelength, B_m^i 、 R_m^i 、 θ_m^i respectively represents

perpendicular baseline, oblique distance, and radar wave perspective at point m on the interferogram.

A local Delaunay triangulation network was established according to the obtained stable high-coherence points, and the initialization parameter solution and refinement parameter solution were performed (ZHANG Ling et al,2014). The relative linear deformation rate and relative elevation error between two points were alculated by the model coherence coefficient. Integrate the relative linear deformation rate and relative elevation error between the two highly coherent points by set a certain high coherence point with known deformation and DEM error as the reference point to obtain the linear deformation rate and nonlinear deformation of each point target. Estimate the corresponding nonlinear deformation of each SAR imaging moment (with the first phase image as time reference) through filtering method of time and space, and accumulate together the linear deformation and the nonlinear deformation to generate the time-series of cumulative deformation at 3-month intervals from January 2017 to September 2020 (see Figure 7). It shows that the subsidence continued to expand from January 2017 to September 2020, while the subsidence development was slow in earlier stage and became obvious until 2020, and the maximum cumulative subsidence reached nearly 30cm.

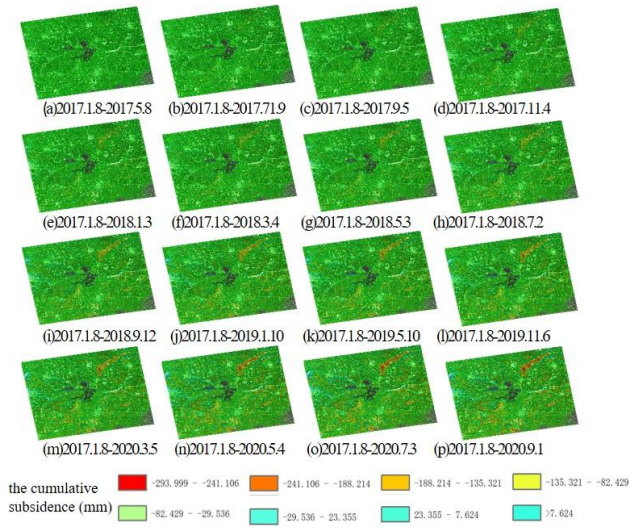

Figure 7. Time-series of cumulative subsidence from January 2017 to September 2020

3.4 Characteristic Deformation Analysis

The deformation rate figure (Figure 8) and the cumulative deformation value figure (Figure 9) about Sentinel-1 data from January 8, 2017 to September 1, 2020 show that obvious subsidence area existed in the northern part of Xiongxian County. Among which, most area of the county (about 70% or more) had slight land subsidence with rate of less than 1cm/yr and cumulative subsidence of less than 3cm. While the most significant subsidence occurred in the northern area, mainly distributed in Daying Town, Xiongzhou Town and other areas. The maximum subsidence rate of those areas was nearly 7cm/yr, and the maximum cumulative subsidence reached 30cm.

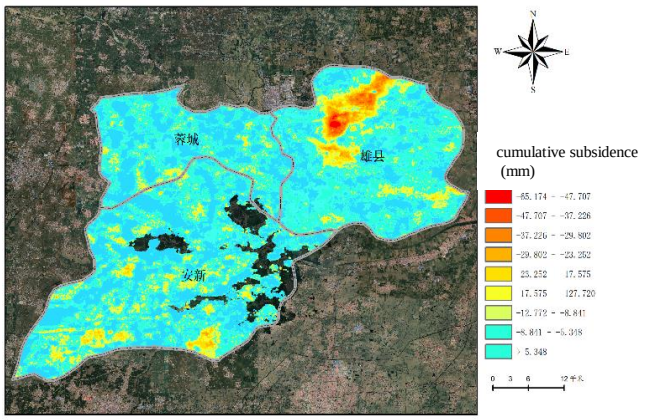

Figure 8. Deformation rate of Xiong'an New Area

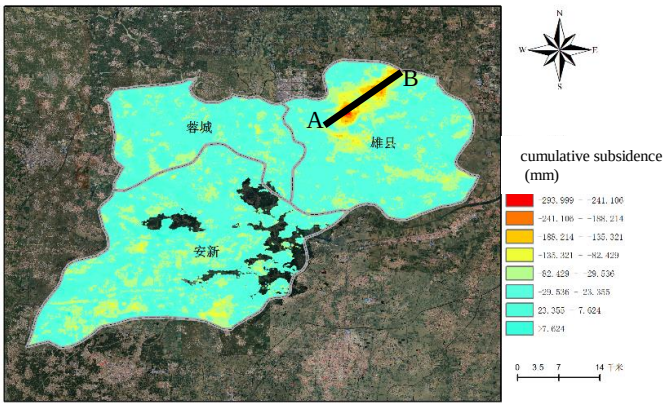

Figure 9. Cumulative deformation of Xiong'an New Area

The comparison of the monitoring results in this paper with relevant literature shows that a clear subsidence trend occurred in the northern area of Xiongxian County with the maximum subsidence rate of 7.5cm/yr during 2012 to 2016 (see Figure 10). It found that the subsidence trend was continued in most area of Xiongxian Couty (70%) in 2017-2020 while put the relevant literature and the research results of this paper together, and the subsidence rate and cumulative subsidence continued to expand. Therefore, Xiong'an area kept a slow and stable subsidence trend during 2012-2020, which was clearer in geothermal fields of Niutuo Town, Xiongxian County, North China Plain. Rich geothermal resources were held under 60% area of Xiongxian County, and have been exploited since 2003. The scale of exploitation has increased with economic development in the past decade, performing the main reason why Xiong'an has been in serious subsidence.

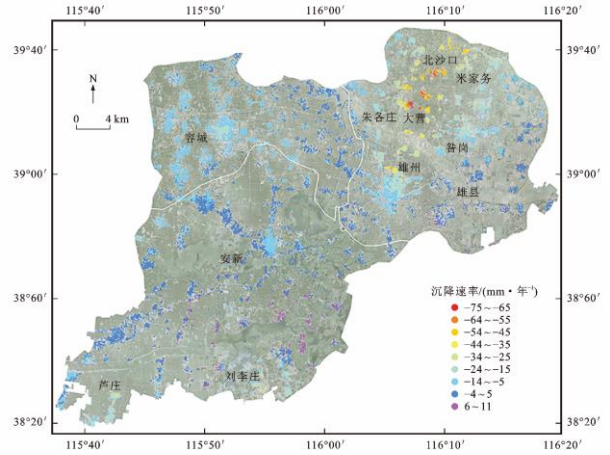

Figure 10. Cumulative subsidence of Xiong'an New Area during 2012-2016

Figure 11 shows the cumulative deformation of the A-B cross-section in the core zone of maximum subsidence. The average subsidence during 2017-2020 in this area was about 10cm, and the maximum subsidence is nearly 25cm.

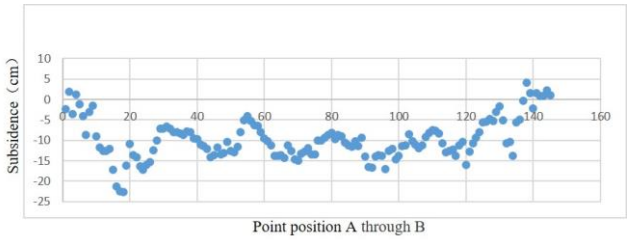

Figure 11. Cumulative deformation of the A-B cross-section

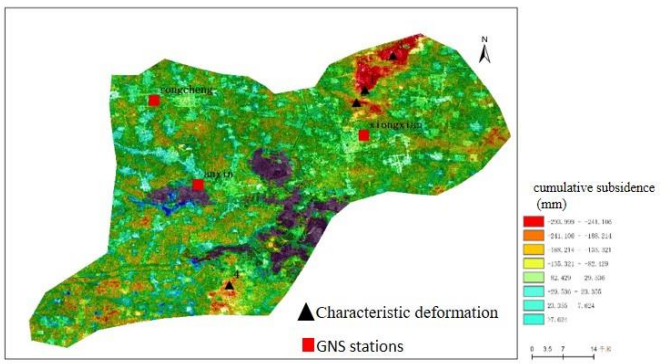

Figure 12. Distribution map of characteristic deformation area and reference station

In Xiong'an New Area, there are three continuously operating reference stations in Xiongxian, Anxin and Rongcheng. According to the monitoring results from Hebei Surveying and Mapping Department, the annual subsidence of each reference station area are -3.15cm, -1.21cm and -1.16cm, respectively. While the annual subsidence of surrounding areas of those three reference stations are about -3.37cm, -1.01cm, and -1.44cm, respectively in accordance with the subsidence rate monitored in this paper (see Figure 8), and the subsidence trend is basically consistent with the subsidence.

Extract four areas with obvious deformation characteristics (area #1, #2, #3 and #4 in Figure 12), such as the northern part of Xiongxian, the southern part of Anxin and other areas with severe subsidence, and conduct subsidence time-series analysis respectively (see Figure 13-20). From the perspective of the spatial distribution of subsidence areas, three areas (#1-3) in the northern part of Xiongxian locate in the area with rich geothermal resource, and #4 area is covered by farmland and needs underwater for irrigation for a long time, which results in obvious subsidence.

The average subsidence rate of the center point of #1 area is 3.24cm/yr, and the maximum cumulative subsidence is nearly 12cm; the average subsidence rate of the center point of #2 area is 3.43cm/yr, and the maximum cumulative subsidence is nearly 15cm; the average subsidence rate of the center point of #3 area is 4.17cm/yr, the maximum cumulative subsidence is nearly 15cm; the average subsidence rate of the center point of #4 area is 3.8cm/ yr, and the maximum cumulative subsidence is nearly 13cm.

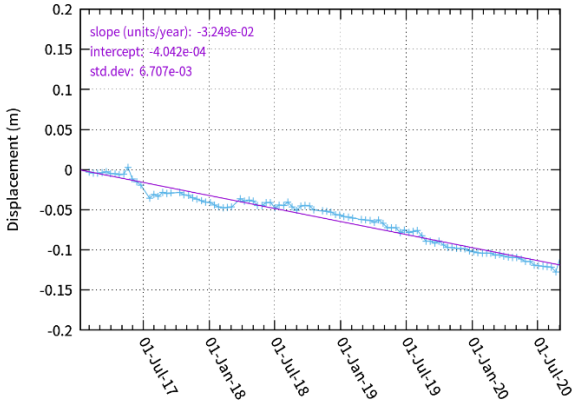

Figure 13. Subsidence line chart of #1 deformation area

Figure 14. Location of #1 deformation area

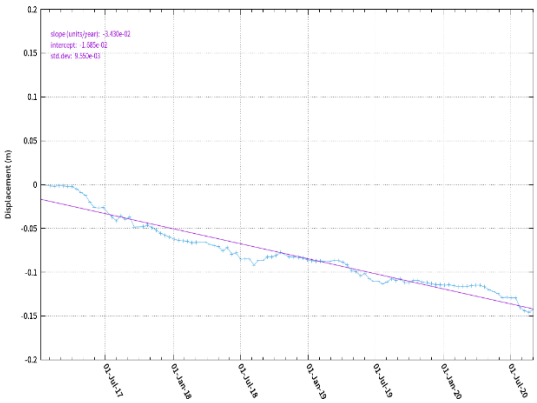

Figure 15. Subsidence line chart of #2 deformation area

Figure 16. Location of #2 deformation area

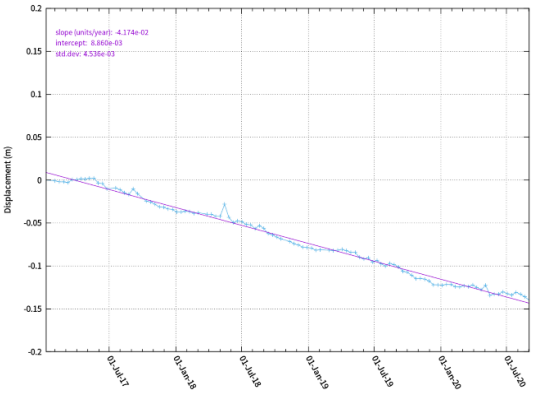

Figure 17. Subsidence line chart of #3 deformation area

Figure 18. Location of #3 deformation area

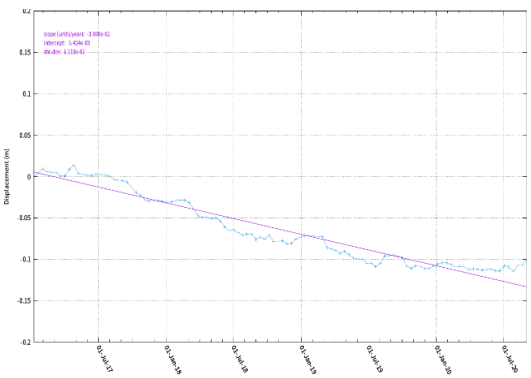

Figure 19. Subsidence line chart of #4 deformation area

Figure 20. Location of #4 deformation area

4. CONCLUSION

This paper extracts the average subsidence rate and cumulative subsidence of Xiaong'an New Area and its surrounding areas from 2017 to 2020 with the 125-scene Sentinel-1 images and with the SBAS-InSAR technology that based on multi-main image coherent targets. It also compares the monitoring results from three continuously operating reference stations with the subsidence rate obtained by InSAR, and those two monitoring results are basically consistent.

More than 70% of the area in the Xiongan New Area has slight subsidence with rate less than 10mm/a. Small land subsidence occurs in Rongcheng County and its surrounding area, while significant land subsidence occurs in some areas of Xiongxian and in the south of Anxin County. On the whole, the areas with relatively serious land subsidence are concentrated in Xiongxian, in where subsidence continues to develop compared with the monitoring results during 2012-2016.

The large-scale subsidence in Xiong'an New Area is mainly caused by multiple factors such as groundwater extraction, geothermal energy exploitation, and underground space construction. With the construction of the new area, more geothermal wells have been dug and mainly located in the northern part of Xiongxian, which is also an important reason for the rapid land subsidence and large cumulative subsidence in the northern part of Xiong'an New Area.

5. ACKNOWLEDGEMENTS

This work was supported by the National Natural Science Foundation of China (No. 41504020) and the National Natural Science Foundation of China (No. 41804038).

6. REFERENCES

ZHANG Y H, ZHANG JX, WU H G, et al., 2011: Monitoring of Urban Subsidence with SAR Interferometric Point Target Analysis: A Case Study in Suzhou, China. International Journal of Applied Earth Observation and Geoinfoemation 13(5), 812-818.

XIONG Peng, ZUO Xiao-qin, LI Yong-fa, et al., 2020: Application of dual-polarized Sentinel-1 data to subsidence monitoring in Kunming. Progress in Geophysics (in Chinese), 35(4), 1317-1322.

XIONG Jiacheng, NIE Yunju, LUO Yue, LI Yongfei, 2019: Monitoring urban land subsidence by dual-polarization Sentinel-1 data: a case study of Shanghai. Bulletin of Surveying and Mapping, 10(11), 98-102, 129.

XIAO Weifeng, YANG Wentao, LI Chaokui, et al., 2020: Detection of Influence Factors and Their Interaction of Land Subsidence in Beijing Based on PS-InSAR. Geomatics World 27(06), 7-13.

Jia Sanman, Tian Fang, Qi Qian, 2019: Urban "chronic diseases"-the cause of land subsidence and comprehensive prevention and control measures. City and Disaster Reduction (3), 22-27.

GAO Ertao, FAN Donglin, FU Bolin et al., 2019: Land Subsidence Monitoring of Nanjing Area Based on PS-InSAR and SBAS Technology. jgg 39(2),158-163.

Wang Xiaoqing, Zhang Peng, et al., 2018: Mitigation Atmospheric Effects in Interferogram With Using Integrated MERIS/MODIS Data and A Case Study Over Southern California. The International Archives of the Photogrammetry, Remote Sensing and Spatial Information Sciences, Volume XLII-3, 2018.

Yang Q, Ke Y, Zhang D, et al., 2018: Multi-scale analysis of the relationship between land subsidence and buildings: A case study in an eastern Beijing Urban Area using the PS-InSAR technique. Remote Sensing 10(7), 1006-1008.

Solari L, Ciampalini A, Raspini F, et al., 2016: PSI-nSAR analysis in the Pisa urban area (Italy): A case study of subsidence related to stratigraphical factors and urbanization. Remote Sensing 8(2), 120-128.

Zhu L, Gong H, Li X, et al., 2015: Land subsidence due to groundwater withdrawal in the northern Beijing plain. Engineering Geology 193, 243-255.

WANG Xiaoqing, DANG Ya-min, ZHANG Peng, et a1., 2012: Application of MERIS atmospheric water vapor to ASAR interferogram correction. Progress in Geophysics 27(6), 2335-2341.

ZHANG Ling, GE Daqing, GUO Xiaofang, et.al., 2014: Land Subsidence in Cangzhou over the last Decade Based on Interferometric Time Series Snalusis. Shanghai Land and Resources 35(4), 72-75,80.